Multi-Layer Phase Analysis: Quantifying the Elastic Properties of Soft Tissues and Live Cells with Ultra-High-Frequency Scanning Acoustic Microscopy

Xuegen Zhao, Riaz Akhtar, Nadja Nijenhuis, Steven J. Wilkinson, Lilli Murphy, Christoph Ballestrem, Michael. J. Sherratt, Rachel E. B. Watson, and Brian Derby

***Abstract*—Scanning acoustic microscopy is potentially a powerful tool for characterizing the elastic properties of soft biological tissues and cells. In this paper, we present a method, multi-layer phase analysis (MLPA), which can be used to extract local speed of sound values, for both thin tissue sections mounted on glass slides and cultured cells grown on cell culture plastic, with a resolution close to 1 μm. The method exploits the phase information that is preserved in the interference between the acoustic wave reflected from the substrate surface and internal reflections from the acoustic lens. In practice, a stack of acoustic images are captured beginning with the acoustic focal point 4 μm above the substrate surface and moving down in 0.1-μm increments. Scanning parameters, such as acoustic wave frequency and gate position, were adjusted to obtain optimal phase and lateral resolution. The data were processed offline to extract the phase information with the contribution of any inclination in the substrate removed before the calculation of sound speed. Here, we apply this approach to both skin sections and fibroblast cells, and compare our data with the $V(f)$ (voltage versus frequency) method that has previously been used for characterization of soft tissues and cells. Compared with the $V(f)$ method, the MPLA method not only reduces signal noise but can be implemented without making *a priori* assumptions with regards to tissue or cell parameters.**

I. Introduction

Changes in the mechanical properties of soft tissues are known to profoundly influence both human morbidity and mortality. The physical properties of skin, for example, are known to change with both chronological age and exposure to environmental factors [1], [2], and increased arterial stiffness, which is associated with age, diabetes, and many other factors, leads to hypertension, stroke, heart failure, and end-stage renal failure [3]–[5]. Hence, there is considerable interest in developing new approaches to characterize the mechanical properties of soft tissues. However, tissues such as skin are highly heterogeneous anisotropic materials whose composition and microscopic structure can vary as a consequence of both age and disease. There is a need therefore, to develop micro-mechanical approaches which, in combination with conventional histochemical methods, can measure the mechanical properties of discrete tissue components [6].

The accurate characterization of the elastic properties of cells is needed to better understand the mechanical function of the cytoskeleton and the response of cells to changes in their local mechanical environment [7]. Improved methods for the measurement of mechanical properties using very small forces and displacements [8] coupled with the development of constitutive models for cell mechanical behavior [9] has led to several studies investigating the mechanical behavior of cells.

Atomic force microscopy (AFM)-based methods are currently the most widely used techniques for the mechanical investigation of soft tissues and cells because they combine a high lateral spatial resolution with good qualitative resolution of mechanical properties. However, it is difficult to quantify sample stiffness from AFM data because the high compliance of both cells and soft tissues limits the applicability of the conventional Hertzian contact mechanics approach [8]. There are further limitations inherent in the technique, such as the difficulty in accurately determining the cantilever spring constant [10]. In addition, for conventional thin histology slices mounted on glass and for cells spread on a substrate, it is difficult to prevent the properties of the substrate from dominating the AFM response [11]. Other techniques such as nanoindentation have a more secure mechanical foundation than AFM, but this accuracy in mechanical property measurement is compromised by a significantly inferior spatial resolution. In addition, the response of the substrate also affects nanoindentation measurements [12]. Finally, when applied to living cells, indentation-based methods mechanically disturb the cytoskeleton cell [13] and hence may induce a mechanical response. Thus, there is a need to develop high-spatial resolution non-contact methods to

Manuscript received June 3, 2011; accepted January 12, 2012. The authors are grateful to the Wellcome Trust (WT085981AIA), BBSRC, AgeUK (Senior Fellowship awarded to MJS: Grant No. 266), and the British Heart Foundation for funding (Advanced Training Award FS/08/036/25364 to RA).

X. Zhao, S. J. Wilkinson, and B. Derby are with and R. Akhtar and L. Murphy were with the School of Materials, The University of Manchester, Manchester, UK.

R. Akhtar was with the Cardiovascular Sciences Research Group, Manchester Academic Health Science Centre, The University of Manchester, Manchester, UK.

R. Akhtar is now with the School of Engineering, University of Liverpool, Liverpool, UK (e-mail: r.akhtar@liverpool.ac.uk).

N. Nijenhuis and C. Ballestrem are with the Faculty of Life Sciences, The University of Manchester, Manchester, UK.

M. J. Sherratt and R. E. B. Watson are with the Faculty of Medical and Human Sciences, Manchester Academic Health Science Centre, The University of Manchester, Manchester, UK.

DOI: http://dx.doi.org/10.1109/TUFFC.2012.2240

accurately characterize the mechanical behavior of cells and soft tissues.

The potential utility of scanning acoustic microscopy (SAM) for biomedical applications [14] has long been recognized and the technique has been used to characterize living cells [15] and soft tissues such as blood vessels [16], [17] and heart valves [18]. The advantages of SAM include relatively fast acquisition, high spatial resolution (around 1 μm at 1 GHz excitation), ease of sample preparation, the ability to obtain histological data (without the need for specific staining), and non-destructive imaging of cells [19]. Although images of cells and tissue sections can be collected relatively easily, quantitative measurements are more challenging than for engineering materials [20] or stiff, calcified tissues [21], which can both be prepared to provide a flat specimen surface. The contrast observed in a SAM image contains complex phase information through the interference of several signals from the specimen and any interface with a significant acoustic impedance mismatch. Fig. 1 shows a schematic of a soft biological specimen mounted on a substrate, immersed in an acoustic coupling fluid (normally distilled water or buffered saline) immediately beneath an acoustic lens. The lens both transmits a short burst of ultra-high frequency acoustic energy and acts as the receiver for the reflected signals. Reflections are generated at all of the interfaces in the system: lens/fluid, fluid/specimen, and specimen/substrate. In addition, Rayleigh waves may radiate along the substrate surface and these leaky Rayleigh waves radiate acoustic energy from the substrate toward the lens. The signal received at the lens thus results from the interference between the reflections and the amplitude determined by the intensities and phase of each wave. Thus, if the lens is moved in the z-direction, normal to the surface, a complex oscillating intensity is recorded, known as the $V(z)$ curve or response [22], [23].

Quantitative analysis of the mechanical properties of specimens in the acoustic microscope is achieved by analyzing the phase information in the reflected signal. In most cases, this is achieved through appropriate gating of the received signal to reduce the number of specimen-related signals, hence simplifying analysis of the $V(z)$ curve to interference between two signals. In the cases of soft tissues on glass slides or cells on substrates, the strong reflection from the substrate is often taken as a suitable reference signal that interferes with the weaker reflection from the specimen fluid interface. It is also possible to investigate the change in amplitude and phase of the reflected signal when the frequency of the acoustic excitation is varied rather than the acoustic path length. This method is known as frequency scanning or the $V(f)$ method [15].

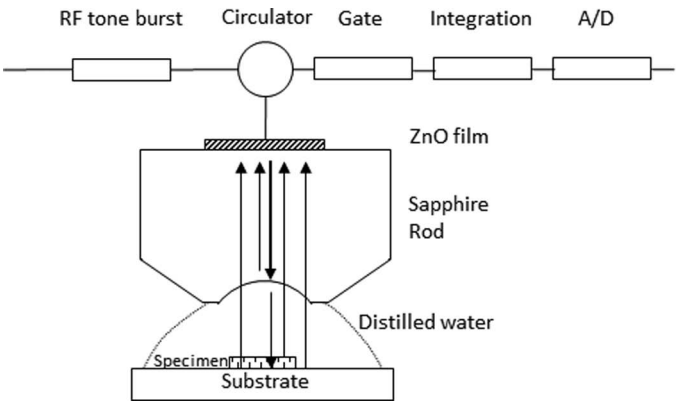

Fig. 1. Schematic representation of the scanning acoustic microscope (SAM). When a sound wave is generated and propagates through the acoustic lens, medium, and specimen, there are reflections from acoustic lens/medium, specimen/medium, specimen/substrate, and medium/substrate interfaces.

Several approaches have been used to determine the properties of biological samples by using SAM and recording the $V(z)$ response [24], [25]. Kundu *et al.* [26], [27] computed the properties of chemically fixed cells by using the simplex algorithm to estimate the cell thickness profile and longitudinal wave speed in the cell. With this information, they estimated the probable upper and lower bounds of the cell thickness at different pixels or cell positions. They developed this method further by comparing synthetically-derived pixel intensities along a line scan with experimental $V(z)$ data, using a simplex inversion algorithm to obtain the best estimate of the unknown values of cell thickness profile, acoustic wave speed, and attenuation at each pixel.

There have also been studies of the properties of cells using the $V(f)$ method [28]. Kundu *et al.* further developed their methods using the signal intensity as a function of frequency, $V(f)$, to obtain the acoustic properties of cells using the simplex algorithm. They have also applied the analysis to soft tissue specimens [18], [29]. The $V(f)$ approach has several advantages over other methods that have been used for characterization of the elastic properties of cells, including the relatively fast acquisition time of a $V(f)$ data set. Recently, we have employed this approach to demonstrate that the gross tissue stiffening which characterizes the aging aorta is localized to collagen fibril-rich regions within the medial layer of the vessel wall [30].

However, although relative differences in speed of sound through cells and tissues can be computed using either of the $V(f)$ methods coupled with algorithmic optimization, the method relies on a defined set of upper and lower bounds before optimization [15]. The resultant wave speed values are found to be highly dependent on the initial bounds that have been defined (possibly arbitrarily). Further, we have found that the sound waves that are reflected from the specimen also interfere with stray echoes inside the acoustic lens. This interference results in a voltage signal that significantly depends on the acoustic frequency and the distance between the lens and the specimen, further complicating the analysis of $V(f)$ data. In light of these confounding issues with current methods of analyzing SAM data for cells and soft tissues, this study had the goal of developing a novel analysis method by utilizing phase information. We have found that the interference between the in-lens echoes and the reflections from the specimen preserves phase (timing) information

and also that this interference can be utilized to determine the acoustic wave speed as well as attenuation in tissues. We have compared our approach to the $V(f)$ method using cells and soft tissues as examples to show the utility of our approach.

II. Methods

A. Cell and Tissue Preparation

NIH 3T3 mouse fibroblasts were plated on polystyrene culture dishes (60-mm-diameter; BD Biosciences, Oxford, UK) coated with 10 μg/mL bovine plasma fibronectin (Sigma-Aldrich Co. LLC, Dorset, UK) and kept overnight in Dulbecco's modified Eagle's medium (DME; Sigma-Aldrich) supplemented with fetal bovine calf serum (FBS; 10%) and L-glutamine (Invitrogen, Life Technologies Corp., Paisley, UK) at 37°C in 5% CO_2.

Histological cryosections (5 μm) of human skin were prepared from a 6-mm-diameter punch biopsy excised from a photoprotected site (buttock) of a 35-year-old female volunteer. The samples were embedded in optimal cutting temperature (OCT) medium (Miles Laboratories, Elkhart, IN), snap-frozen in liquid N_2, and immediately stored at −80°C pending cryosectioning, when samples were mounted on glass slides.

B. Scanning Acoustic Microscopy

The method outlined in this study was developed on a KSI 2000 microscope (PVA TePla Analytical Systems GmbH, Herborn, Germany) modified with a custom data acquisition and control system. A similar system has been described in detail by Raum [21] and is schematically shown in Fig. 1. In brief, the system operates at two frequency regimes; at frequencies up to 400 MHz, the acoustic lenses are excited with a short pulse, with a pulse width of around 1 ns, and at frequencies between 800 MHz and 2 GHz (which is the regime we have worked with), the lenses are excited with quasi-monochromatic tone bursts, with burst length of around 20 ns and a repetition rate of approximately 500 kHz.

The acoustic lens has a plano-concave design consisting of a sapphire cylindrical rod with a zinc oxide piezoelectric film deposited on one end as the transducer and a spherical cavity on the other end acting as an acoustic lens. For the 1-GHz lens used in this investigation, the cavity has an aperture of 80 μm in diameter and an included angle of 100°. The specimen was placed on a horizontal stage and scanned by the lens. An aqueous fluid provides acoustic coupling between the lens and the specimen; Ham's F12 medium (Sigma-Aldrich) was used for the cells and distilled water was used for the tissue samples.

All of the SAM experiments were conducted in an air-conditioned laboratory and minimal temperature fluctuations were expected during the course of the experiments because the laboratory temperature was found to be very stable during the course of the experiments. It is extremely difficult to directly measure the temperature distribution in the focal area of the acoustic lens [31], however, we recorded the temperature of the coupling fluid, measured by a Digitron 2038T thermometer with a Type-K thermocouple (Digitron Instrumentation Ltd., Devon, UK). The temperature was typically 23°C, with maximum variation over 1 h being ±0.1°C.

The power transferred to the sample during acoustic microscopy is believed to be extremely small (fractions of a miliwatt). This is supported by theoretical calculations, which suggest that any temperature increase during acoustic microscopy is small [31], [32]. Weiss *et al.* [33] have suggested that there are no biological effects of temperature fluctuations caused by ultrasound in cells. Our measurements of coupling fluid temperature further suggest that the heating effect caused by the absorption of acoustic energy is negligible for the type of instrument utilized in this study. Our measurements of coupling fluid temperature change, as indicated previously, found a temperature variation of ± 0.1°C during a typical experimental run time. The speed of sound in water is known to vary by about 2.8 $m{\cdot}s^{-1}$ per 1°C change in temperature [34], thus we anticipate any uncertainty in our speed of sound measurements caused by variation in sample or coupling fluid temperature to be <1 $m{\cdot}s^{-1}$. This uncertainty is considerably smaller than the typical speed of sound variation in our experimental data and can be ignored.

During operation, acoustic waves travel through the sapphire wave guide and are focused by the acoustic lens. The focused acoustic beam propagates through the coupling fluid and the specimen before reaching the substrate. Reflections occur at the lens/medium, medium/tissue, and tissue/substrate interfaces as a result of the mismatch of acoustic impedances (Fig. 1). The time delay and amplitude of the reflections provide information about the acoustic wave speed and attenuation in the specimen. The reflected waves are received by the same transducer and converted into electrical signals. A 20-ns time window (gate) with variable time delay (gate position) is used as a temporal filter to allow specific signals to pass. After being amplified and integrated, these signals produce a single voltage signal proportional to the amplitude of the reflection that is then converted by a 500 ksample/s analog-to-digital converter card (USB-9201, National Instruments UK, Berkshire, UK) with 12-bit resolution.

With this system, the lens is scanned horizontally in the x- and y-directions by a pair of oscillator coil drives to produce C-mode 2-D images. The fast xy scanner is used to generate C-scan 512 × 512 pixel images with a scan area of 200 × 200 μm; images are collected in approximately 10 s. The z-stage allows the lens–sample distance to be varied at increments as small as 0.1 μm. The MATSAM software (Q-BAM Laboratory, Halle, Germany) that is used to control the system allows a series of C-scan images to be collected at incrementally decreasing lens-sample distances [multilayer analysis (MLA)] [35].

C. Multi-Layer Phase Analysis (MLPA)

In each case, the lens was initially focused at the surface of the substrate (the polystyrene culture dish for cells or glass slide for the tissue sample) by monitoring the maximum output of the received signal with a gate setting optimized for in-focus signals. The lens was then raised 4 μm away from the substrate and an image stack was taken at different z-positions moving from this height toward the substrate surface with a step size of 0.1 μm over a range of 5 μm [Fig. 2(a)]. Scanning parameters, namely acoustic frequency and gate position, were optimized for signal level and lateral resolution.

Following acquisition, the images were processed off-line with custom software developed with Labview (National Instruments UK). The grayscale value for each pixel (x, y position) was extracted from all of the images at each z position to form a $V(z)$ curve. The $V(z)$ data were filtered to remove the subtly changing background and the remaining oscillation components were tapered with a Hanning window followed by fast Fourier transformation (FFT). The single frequency corresponding to the interpolated maximum amplitude was chosen as the spatial frequency v_{osc} of the oscillation and the phase value φ_{osc} of the oscillation was similarly determined [36], [37]. A 2-D phase array was then recovered for the image; this was processed and used to calculate speed of sound. To determine the strength of transmission (inverse of attenuation) of the acoustic wave through the specimen, the maximum of the $V(z)$ curve was used as the sum of all reflections and the average of the weakest $V(z)$ curve (where the amplitude of oscillation is lower than its average) was taken as the contribution of the in-lens echo. The MLPA method is summarized in Fig. 2(b).

It should be noted that the term multi-layer is used here to refer to the method of data acquisition which is based on the MLA method [35] and not on the off-line processing of the data, in which the sum of all the reflections from a single layer is assumed.

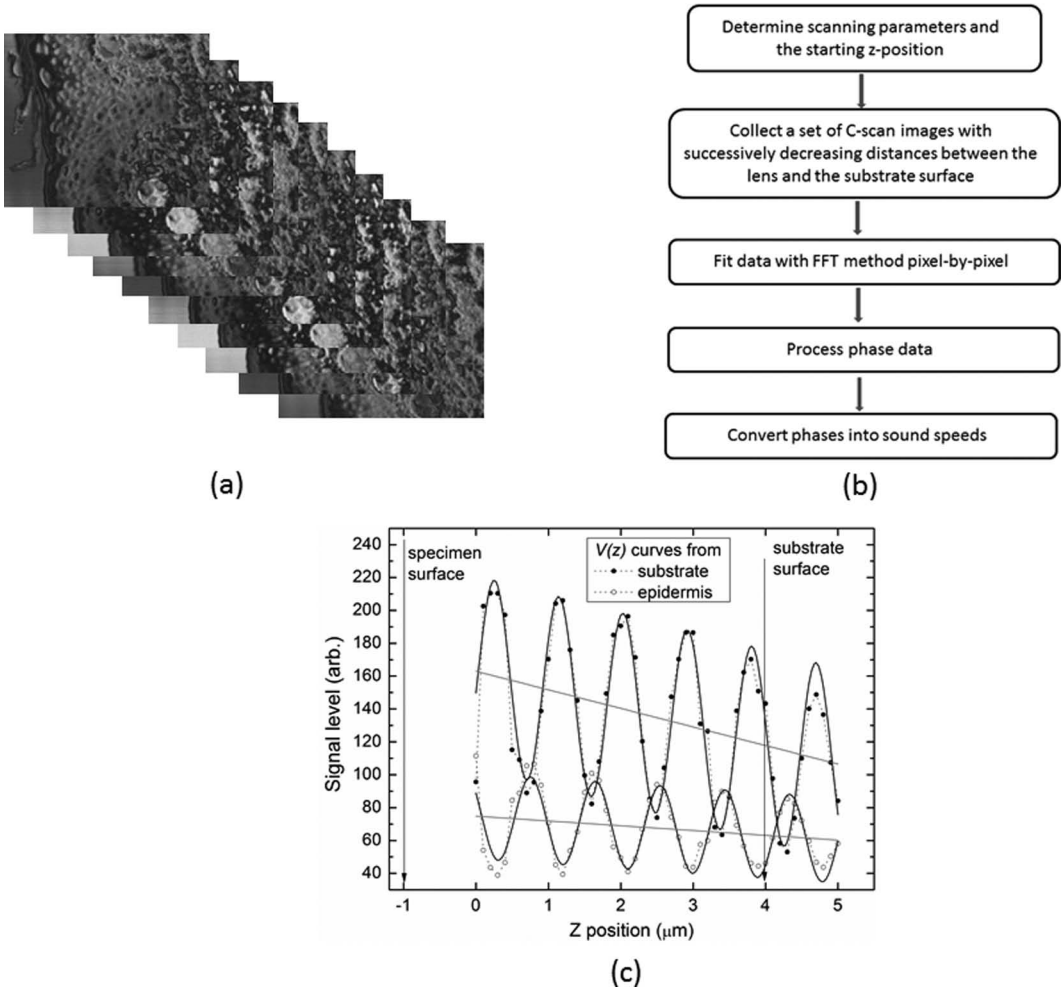

Fig. 2. (a) A stack of images is collected with the multi-layer phase analysis (MLPA) method at 0.1-μm increments starting at a z-position 4 μm above the substrate. (b) Summary of data acquisition and off-line analysis for the MLPA method. (c) $V(z)$ curves shown for different pixel positions from a stack of C-scan images obtained for a skin sample. Periodic oscillations are seen for both the substrate and for the region of tissue sampled (epidermal layer of the skin). The gray lines indicate the linear components (background) of the $V(z)$ curves. The solid curves show the results of fast Fourier transformation (FFT) fitting; the z-position at 0 represents the starting position. The arrows at −1 and 4 μm indicate the positions of specimen surface and substrate surface, respectively.

III. Results

A. Phase Analysis of Acoustic Images

Fig. 2(c) shows two $V(z)$ curves extracted at different pixel positions from a stack of C-scan images [Fig 2(a)] taken from a skin sample. Each curve is composed of an oscillation superimposed over a smooth background. For the $V(z)$ curve of the substrate, the background represents the reflection from the substrate surface (glass slide), and the oscillations indicate the presence of interference with in-lens echoes. However, for the $V(z)$ curve from the tissue, the oscillations represent the sum of all reflections traveling through the tissue and the background indicates the in-lens signal.

When the acoustic beam passes through the specimen and is focused on the substrate surface, the reflected wave reaches its maximum amplitude and any signal from the tissue surface (sample/fluid interface) is relatively weak, if not negligible, because the impedance mismatch is much lower than at the specimen/substrate interface. However, there are also echoes within the lens itself. Such waves can travel between the acoustic lens and zinc oxide film (transducer) many times because of the low attenuation within the sapphire buffer rod, and generate a sequence of electrical pulses at the transducer. This is illustrated in Fig. 3, where in-lens echoes, either strong or weak, can be clearly identified. If appropriate gate settings are selected (e.g., around gate 82 in Fig. 3) interference occurs between the stray in-lens echo and the reflections from the specimen, which preserves relative timing information. The in-lens signal can therefore be used as a timing reference and the timing information (difference in phase) can be extracted from the gated $V(z)$ response.

Assuming the reflections are expressed as $Ae^{i\omega t}$ for the in-lens echo and $Be^{i(\omega t+\varphi)}$ from any of the interfaces, the final wave that reaches the transducer is

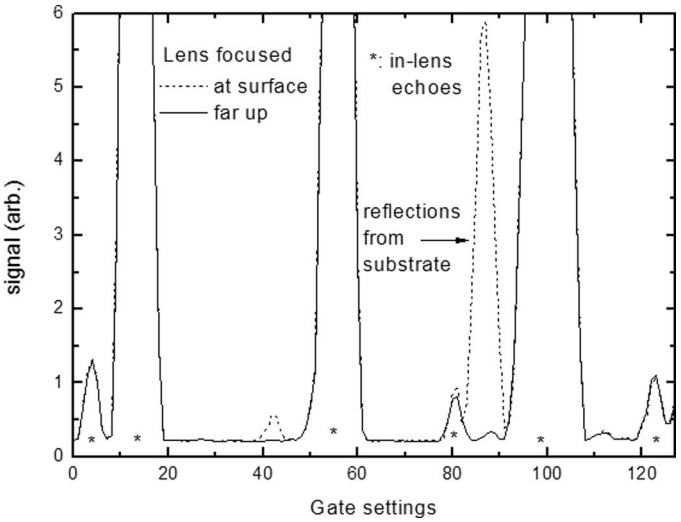

Fig. 3. Signal intensity shown as a function of the lens gate settings. Even when the lens is focused at some distance from the sample surface, strong echoes, which originate from within the lens, can be identified.

$$Ce^{i(\omega t+\gamma)} = Ae^{i\omega t} + Be^{i(\omega t+\phi)}, \tag{1}$$

with the new phase

$$\gamma = \tan^{-1}\frac{A + B\cos\varphi}{B\sin\varphi} \tag{2}$$

and the new amplitude

$$C = \sqrt{A^2 + B^2 + 2A * B * \cos(\varphi)}. \tag{3}$$

Eq. (3) demonstrates that the new amplitude is clearly a function of the phase difference φ. It is obvious that $C = A + B$ when the phase difference is $2n\pi$, and $C = A - B$ when the phase difference is $(2n + 1)\pi$, where n is an integer number. Normally, when the exciting frequency and delay-time window are selected, the phase and amplitude of the in-lens echo will no longer change. However, the amplitude B of the reflected wave is a function of attenuation, and consequently the phase value φ cannot be obtained directly from the detected amplitude C without knowing B. This problem can be overcome by moving the lens in the z direction, and because phase φ is a function of lens position with $\Delta\varphi = 2\pi * 2\Delta z * f/(c_{\text{medium}})$, where f is the frequency of the acoustic signal and c_{medium} is the acoustic wave speed in the coupling media, a periodic oscillation in the recorded voltage signals can be easily obtained with a $V(z)$ scan. However, when the focus of the acoustic beam is far from the substrate surface or the attenuation of the specimen is high, reflections from the specimen/substrate and specimen/fluid interfaces could be comparable in amplitude and interfere significantly when overlapped in the time domain, which makes interpreting the $V(z)$ curve more complicated. To characterize biological tissues and cells, only the interference between the reflection from the specimen/substrate interface and the in-lens echo is desired for calculating sound speed. To minimize the contribution from the specimen/fluid interface, we first use a 20-ns time window to select the time-specific waveform to be processed (i.e., mostly the reflection from the substrate surface, because these two reflections reach the transducer with a difference in time). Next, the acoustic lens is positioned with the focus point beneath the specimen surface and near to the specimen/substrate interface, enhancing the reflection from the substrate surface and, meanwhile, resulting in negligible contribution of surface waves; this differs from a standard $V(z)$ scan in which the acoustic lens is focused deep into the substrate to make use of excited surface waves [23].

B. MLPA Applied to Soft Tissue Sections

Fig. 4 shows images for the skin sample which are generated following pixel-by-pixel processing of the images. Together with the reconstructed transmission image [Fig. 4(b)], a 2-D phase array is recovered and a gray scale image is generated [Fig. 4(c)]. Because of the intrinsic properties of FFT, the recovered phase is limited to within $\pm\pi$,

which introduces discontinuities into the image when the actual phase is beyond this limit. To unwrap these discontinuities, an appropriate integer multiple of 2π is added to each pixel element of the recovered phase map which can then be converted to a speed of sound map [Fig. 4(d)]. In practice, the phase values may need to be adjusted accordingly to reflect the continuity of the specimen, especially at locations where the mechanical properties change significantly. For skin, such a change may be seen in the cornified layer (stratum corneum) as compared with other regions of the epidermis. Furthermore, a change in relative lens-surface distance, either caused by an inclined substrate surface or uneven x-y scanning contour can contribute to the recovered phase value, and such contribution should be removed before further processing. Normally, this can be done by simply subtracting the phase image of the interested area with another phase image obtained from a nearby exposed substrate area with the assumption that the two areas are parallel to each other.

C. Speed of Sound Calculation from Phase Data

The spatial frequency of the oscillation, determined from a $V(z)$ curve, is denoted v_{osc}, and the phases of the oscillation for $V(z)$ curves taken from the exposed substrate surface and from the tissue specimen are denoted $\varphi_{\text{osc-sub}}$ and $\varphi_{\text{osc-tissue}}$, respectively. The following relations hold:

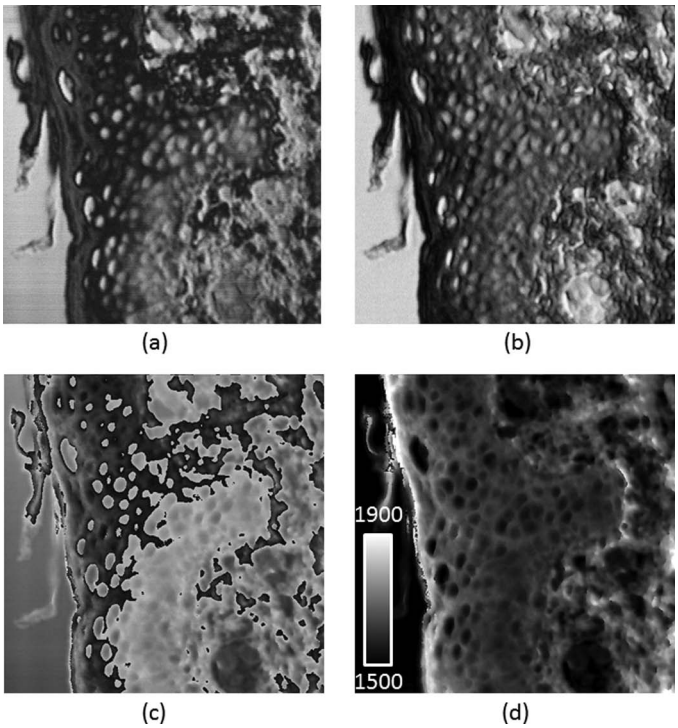

Fig. 4. 200 × 200 μm images of a section of human skin: (a) typical scanning acoustic microscope (SAM) image collected at 1 GHz, (b) reconstructed transmission image, (c) a 2-D phase array is recovered and a gray scale image is generated, and (d) speed of sound map generated from the phase data. The scale ranges from 1500 to 1900 m·s^{-1}.

$$\frac{1}{v_{\text{osc}}} = \frac{c_{\text{medium}}}{2f} \tag{4}$$

$$\varphi_{\text{osc-tissue}} - \varphi_{\text{osc-sub}} = 2\pi f\left(\frac{2d}{c_{\text{medium}}} - \frac{2d}{c_{\text{tissue}}}\right), \tag{5}$$

where d is the tissue thickness, and c_{medium} and c_{tissue} are the sound speeds in the coupling medium and the tissue respectively, and f is the acoustic wave frequency.

Eqs. (4) and (5) can be rewritten to determine the speed of sound in the sample:

$$c_{\text{tissue}} = \frac{4\pi df}{2\pi d v_{\text{osc}} - (\varphi_{\text{osc-tissue}} - \varphi_{\text{osc-sub}})}. \tag{6}$$

An example line profile for skin is shown in Fig. 5; the variation in speed of sound is evident across the line.

D. Comparison of MLPA With the V(f) Method for Cells

We use the example of measuring the acoustic wave speed in a well-adhered cell to compare MLPA with the frequency scanning or $V(f)$ method using SAM. A single mouse fibroblast cell, well-adhered to a polystyrene substrate, was identified in culture and imaged in the SAM. Fig. 6(a) shows a typical SAM image of the cell obtained at a frequency of 1 GHz, showing concentric interference fringes caused by variation in thickness from the cell edge to center.

A series of 6 images of the cell were obtained at 10-MHz intervals in the frequency range 960 to 1010 MHz. To compare the analysis methods, a further series of 50 images were obtained at 0.1-μm increments along the z-axis at a fixed frequency of 1 GHz. These two data sets were then processed using the $V(f)$ method and the MLPA method, respectively.

Fig. 6(b) shows the computed speed of sound across the cell nucleus [marked as the line on Fig. 6(a)] using the $V(f)$ method with the boundary values given in Table I. The result was very noisy and was smoothed by adjacent averaging with the data binned every 10 pixels. Using the unsmoothed data, the average speed of sound through the center of the cell was 1584 ± 8 m·s^{-1}.

Fig. 6(c) shows the phase data calculated from the image stack using the MLPA method, across the same marked region that was analyzed using the $V(f)$ method. The mean speed of sound across the cell nucleus was computed from this data and is presented in Fig. 6(d). On

TABLE I. BOUNDS UTILIZED FOR $V(f)$ ANALYSIS OF AN NIH3T3 CELL.

Parameter	Absolute bounds	Probable bounds
Speed of sound (m·s^{-1})	1450–1700	1500–1650
Cell thickness (μm)	0–5	0.01–4
Cell density (g·cm^{-3})	0.9–1.3	1–1.12

Absolute and probable boundary values were defined as outlined in [16].

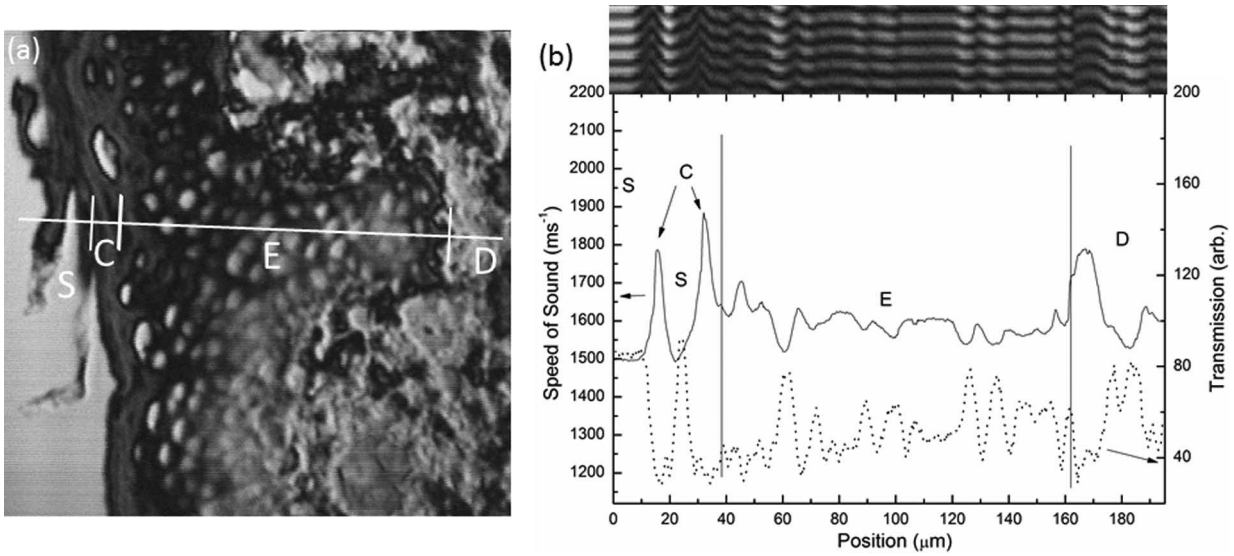

Fig. 5. Scanning acoustic microscope (SAM) image showing a line profile through the different histological layers of the skin: S = glass substrate, C = cornified layer, E = epidermis, and D = dermis. (b) Speed of sound (solid line) and transmission signal (dotted line) values shown across these layers. Inset: reconstructed $V(x, z)$ image.

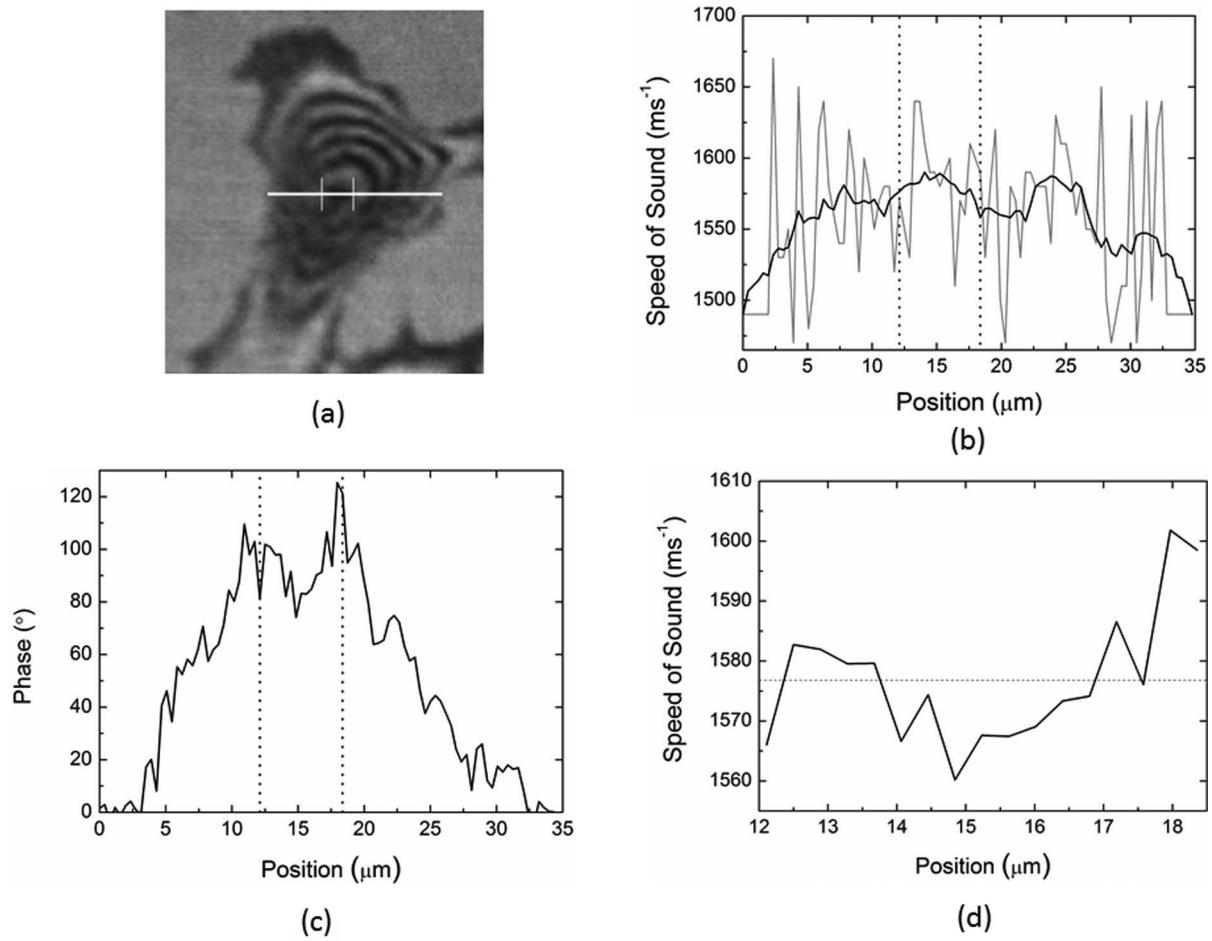

Fig. 6. Comparison of $V(f)$ and multi-layer phase analysis (MLPA) for cells. (a) Typical scanning acoustic microscope (SAM) image of an NIH3T3 mouse fibroblast with line profile marked for analysis. (b) Speed of sound as a function of position using the $V(f)$ method. The gray line shows the actual values, with the smoothed data shown in black. (c) Phase value as a function of position and (d) speed of sound determined from the phase data using the MLPA method.

TABLE II. DIFFERENT BOUNDS FOR SPEED OF SOUND DETERMINATION WITH $V(F)$ FOR CELLS.

Absolute bounds	Probable bounds	Speed of sound ($m \cdot s^{-1}$)
Speed of sound		
1450–1700	1500–1650	1584 ± 8
1450–1650	1500–1600	1546 ± 6
1450–1700	1500–1600	1549 ± 9
1500–1700	1550–1650	1599 ± 9
1550–1700	1600–1650	1664 ± 6
Cell thickness		
0–5	0.01–4	1584 ± 8
2–5	3–4	1576 ± 1
2.5–5	3–4	1598 ± 1

TABLE III. DIFFERENT BOUNDS FOR SPEED OF SOUND DETERMINATION FOR SKIN SAMPLE WITH $V(F)$.

Absolute bounds	Probable bounds	Speed of sound ($m \cdot s^{-1}$)
1400–1800	1500–1750	1666 ± 5
1400–1750	1500–1700	1622 ± 5
1400–1800	1500–1700	1624 ± 5
1450–1800	1550–1750	1695 ± 4
1500–1800	1600–1750	1698 ± 3

comparison with Fig. 6(b), it is clear that this method (using a constant frequency) produces data with considerably less noise. The average speed of sound across the nucleus region using the MLPA method was 1577 ± 3 $m \cdot s^{-1}$.

At first it appears that the two methods of analyzing the SAM data produce similar values. However, further investigation of the $V(f)$ method showed it to be highly sensitive to the initial boundary values used. The influence of the initial boundary values of speed of sound on the computed optimized speed of sound using the $V(f)$ method is demonstrated in Table II. The final optimized speed of sound is seen to be extremely sensitive to the bounding values, with the range of computed speed of sound values being significantly greater than the experimental scatter. The influence of the boundary values of specimen thickness (Table II) is less marked than that for speed of sound but is at least comparable, if not greater than the experimental scatter.

It appears that the limited number of data points utilized by the $V(f)$ method and the large number of starting parameters that must be optimized result in estimated speed of sound values that are highly dependent on the upper and lower bounds.

To some extent, the influence of specimen thickness bounds can be alleviated by inspecting the image of the cell [Fig. 6(a)] and using the interference fringes to define realistic bounds at each location on the cell. However, the need for operator intervention reduces the utility of the $V(f)$ approach to determine cell properties from SAM data.

E. Comparison of MLPA With the V(f) Method for Skin Cryosections

A similar comparison between the two analysis methods can be carried out using skin samples. Fig. 7 shows $V(f)$ data alongside MLPA data for skin sections from the same donor and anatomical site. The raw line profile data from the $V(f)$ method is very noisy [Fig. 7(b)], as was the case with the cell sample [Fig. 6(b)], and requires smoothing. The MLPA data are much less noisy [Fig. 7(c)]. Furthermore, the variation in speed of sound data across histological layers is much clearer with the MLPA approach (e.g., the large difference in speed of sound between the cornified layer and rest of the epidermis).

When comparing the data extracted from the SAM images of cells, the optimized speed of sound value determined using the $V(f)$ method is very sensitive to the initial bounding values. In the case of thin histological specimens it was not possible to obtain an independent estimate of sample thickness, as was available from counting the interference rings on the cell specimen. It is possible to estimate bounds for the acoustic wave speed values using data in the literature, e.g., the values recorded by Moran [38], or through the use of reference tables [39]. Table III shows how changing the input bounds in the $V(f)$ analysis alter the estimated speed of sound in the skin sample. As was the case with the cell analysis, the variation in value is much greater than the statistical scatter across a specimen.

The accuracy of the speed of sound measurements is generally governed by the speed of sound in the reference medium, the accuracy of specimen thickness, and the accuracy of measuring the time differences in the acoustic signals [38]. For the $V(f)$ method, the specimen thickness is the most important criteria for determining reliable speed of sound values (Table II).

This is more critical for soft tissues, because with cells, counting interference rings can be used to determine their thickness. For soft tissues, the nominal thickness to which the tissues have been sectioned must be relied on. However, Fig. 8 demonstrates that with the MLPA approach, the error in the speed of sound values when the specimen thickness is under or overestimated for a soft tissue section is small, particularly when the phase difference is low; e.g., if the actual thickness of a tissue section is 6 μm and the thickness value used is ±1 μm. In our case, tissues were sectioned at a thickness of 5 μm. For soft tissues such as skin, which was imaged in this study, phase values are around 300°, compared with 100° for cells.

Fig. 8 demonstrates that an under- or overestimation of this thickness gives rise to only a small error in speed of sound when using the MLPA method. Accurate thickness measurements are more critical for thinner sections or when the phase difference is high. The $V(f)$ method introduces the additional problem of determining suitable absolute and probable bounds before estimation of speed of sound values. In addition, the $V(f)$ method assumes that the focal position is determined with a high accuracy, which is difficult to achieve in practice [33].

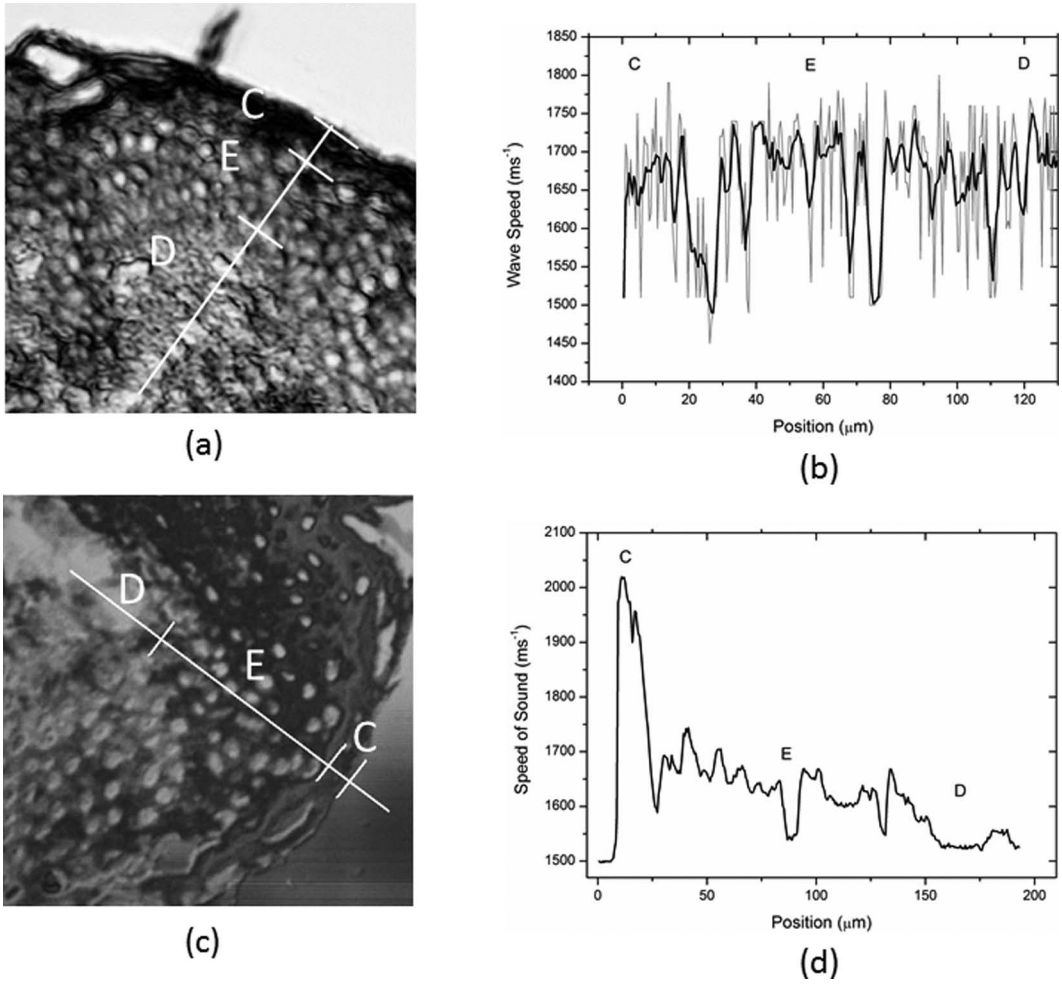

Fig. 7. Comparison of $V(f)$ and multi-layer phase analysis (MLPA) for skin. (a) Typical scanning acoustic microscope (SAM) image collected with the $V(f)$ method with line profile marked for analysis. (b) Sound speed as a function of position determined with the $V(f)$ method. The gray line shows the actual values, with the smoothed data shown in black. (c) Typical image from MLPA stack and (d) sound speed profile determined using the MLPA method. The data collected with the MLPA method is less noisy and shows a clear transition in sound speed from the cornified layer (C) through to the epidermis (E) and dermis (D).

Phase imaging with SAM has been used previously for thin film characterization because this yields additional information that cannot be extracted from acoustic amplitude images alone [40], [41]. We now combine multilayer analysis [21] with phase analysis; with our approach, the method becomes an extremely powerful tool for locally (~1 μm spatial resolution) characterizing the speed of sound in cells and soft tissues. However, the acquisition times per data set under the current MLPA method are relatively long compared with the $V(f)$ method. For the data presented in this paper, acquisition of the $V(z)$ image stack took around 13 min: the image stack was composed of 50 images with a 5-μm change in z-position and a 0.1-μm z-axis step size. In contrast, with the $V(f)$ method, often approximately 6 images are recorded at incrementally increasing frequencies [18], thereby resulting in an acquisition time of approximately 1 min with a 200 × 200 μm scan field and 512 × 512 pixel resolution.

Although the acquisition time is not a limiting factor for the characterization of soft tissues, it is an important factor if SAM is to be used as a time-resolved tool for cell biology where the temporal resolution of a migrating

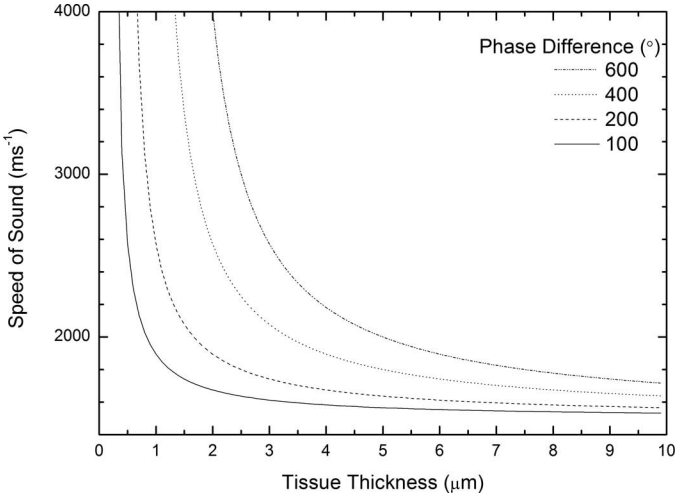

Fig. 8. The absolute error is dependent on the thickness value that is used in (6). Speed of sound variation with different input thickness values is demonstrated here. The error in the speed of sound values decreases with thicker sections or when there is a smaller phase difference.

cell may be important [11]. In such instances, the MLPA method may require further development, such as using lower image resolution to reduce the total time required, or a modified protocol for the MLPA method, e.g., determining a lower bound to the number of images required for accurate analysis.

III. Conclusions

We presented a new quantitative analysis method for ultra-high frequency SAM which is suitable for determining the elastic properties of soft tissues and cells. This approach, the MLPA method, exploits the phase information that is preserved in the interference between an acoustic wave reflected from the substrate surface and internal reflections from the acoustic lens.

Acknowledgments

The authors would like to thank Dr. S. Brand (Fraunhofer Institute of Material Mechanics, Germany) and Professor K. Raum (Julius Wolff Institut and the Berlin-Brandenburg School for Regenerative Therapies, Germany) who developed the MATSAM software used to collect the acoustic images and Dr. C. Riis (Aarhus University Hospital, Denmark) who kindly provided access to the STAN software used for $V(f)$ analysis.

References

[1] E. C. Naylor, R. E. B. Watson, and M. J. Sherratt, "Molecular aspects of skin ageing," *Maturitas*, vol. 69, no. 3, pp. 249–256, 2011.
[2] M. J. Sherratt, "Tissue elasticity and the ageing elastic fibre," *Age*, vol. 31, pp. 305–325, Dec. 2009.
[3] P. Boutouyrie, A. I. Tropeano, R. Asmar, I. Gautier, A. Benetos, P. Lacolley, and S. Laurent, "Aortic stiffness is an independent predictor of primary coronary events in hypertensive patients—A longitudinal study," *Hypertension*, vol. 39, pp. 10–15, Jan. 2002.
[4] S. Aoun, J. Blacher, M. E. Safar, and J. J. Mourad, "Diabetes mellitus and renal failure: Effects on large artery stiffness," *J. Hum. Hypertens.*, vol. 15, pp. 693–700, Oct. 2001.
[5] K. Cruickshank, L. Riste, S. G. Anderson, J. S. Wright, G. Dunn, and R. G. Gosling, "Aortic pulse-wave velocity and its relationship to mortality in diabetes and glucose intolerance—An integrated index of vascular function?" *Circulation*, vol. 106, pp. 2085–2090, Oct. 2002.
[6] R. Akhtar, M. J. Sherratt, J. K. Cruickshank, and B. Derby, "Characterizing the elastic properties of tissues," *Mater. Today*, vol. 14, no. 3, pp. 96–105, 2011.
[7] S. Suresh, "Biomechanics and biophysics of cancer cells," *Acta Biomater.*, vol. 3, pp. 413–438, Jul. 2007.
[8] K. J. Van Vliet, G. Bao, and S. Suresh, "The biomechanics toolbox: Experimental approaches for living cells and biomolecules," *Acta Mater.*, vol. 51, pp. 5881–5905, Nov. 2003.
[9] C. T. Lim, E. H. Zhou, A. Li, S. R. K. Vedula, and H. X. Fu, "Experimental techniques for single cell and single molecule biomechanics," *Mater. Sci. Eng. C*, vol. 26, pp. 1278–1288, Sep. 2006.
[10] D. Kirmizis and S. Logothetidis, "Atomic force microscopy probing in the measurement of cell mechanics," *Int. J. Nanomedicine*, vol. 5, pp. 137–145, Apr. 2010.
[11] H. D. Liang and M. J. K. Blomley, "The role of ultrasound in molecular imaging," *Br. J. Radiol.*, vol. 76, spec. no. 2, pp. S140–S150, 2003.
[12] R. Akhtar, N. Schwarzer, M. J. Sherratt, R. E. B. Watson, H. K. Graham, A. W. Trafford, P. M. Mummery, and B. Derby, "Nanoindentation of histological specimens: Mapping the elastic properties of soft tissues," *J. Mater. Res.*, vol. 24, pp. 638–646, Mar. 2009.
[13] G. T. Charras and M. A. Horton, "Single cell mechanotransduction and its modulation analyzed by atomic force microscope indentation," *Biophys. J.*, vol. 82, pp. 2970–2981, Jun. 2002.
[14] C. M. W. Daft and G. A. D. Briggs, "The elastic microstructure of various tissues," *J. Acoust. Soc. Am.*, vol. 85, pp. 416–422, Jan. 1989.
[15] T. Kundu, J. Bereiter-Hahn, and I. Karl, "Cell property determination from the acoustic microscope generated voltage versus frequency curves," *Biophys. J.*, vol. 78, pp. 2270–2279, May 2000.
[16] Y. Saijo, T. Ohashi, H. Sasaki, M. Sato, C. S. Jorgensen, and S. I. Nitta, "Application of scanning acoustic microscopy for assessing stress distribution in atherosclerotic plaque," *Ann. Biomed. Eng.*, vol. 29, pp. 1048–1053, Dec. 2001.
[17] Y. Saijo, C. S. Jorgensen, P. Mondek, V. Sefranek, and W. Paaske, "Acoustic inhomogeneity of carotid arterial plaques determined by GHz frequency range acoustic microscopy," *Ultrasound Med. Biol.*, vol. 28, pp. 933–937, Jul. 2002.
[18] A. S. Jensen, U. Baandrup, J. M. Hasenkam, T. Kundu, and C. S. Jorgensen, "Distribution of the microelastic properties within the human anterior mitral leaflet," *Ultrasound Med. Biol.*, vol. 32, pp. 1943–1948, Dec. 2006.
[19] J. Bereiter-Hahn, I. Karl, H. Luers, and M. Voth, "Mechanical basis of cell shape: Investigations with the scanning acoustic microscope," *Biochem. Cell Biol.*, vol. 73, pp. 337–348, Jul.–Aug. 1995.
[20] O. Goodman and B. Derby, "The mechanical properties of float glass surfaces measured by nanoindentation and acoustic microscopy," *Acta Mater.*, vol. 59, pp. 1790–1799, Feb. 2011.
[21] K. Raum, "Microelastic imaging of bone," *IEEE Trans. Ultrason. Ferroelectr. Freq. Control*, vol. 55, pp. 1417–1431, Jul. 2008.
[22] G. A. D. Briggs, *An Introduction to Scanning Acoustic Microscopy*. New York, NY: Oxford University Press, 1985.
[23] J. Kushibiki and N. Chubachi, "Material characterization by line-focus-beam acoustic microscope," *IEEE Trans. Sonics Ultrason.*, vol. 32, no. 2, pp. 189–212, 1985.
[24] H. Sasaki, Y. Saijo, M. Tanaka, H. Okawai, Y. Terasawa, T. Yambe, and S. Nitta, "Influence of tissue preparation on the high-frequency acoustic properties of normal kidney tissue," *Ultrasound Med. Biol.*, vol. 22, no. 9, pp. 1261–1265, 1996.
[25] A. Kamanyi, W. Ngwa, T. Betz, R. Wannemacher, and W. Grill, "Combined phase-sensitive acoustic microscopy and confocal laser scanning microscopy," *Ultrasonics*, vol. 44, pp. E1295–E1300, Dec. 2006.
[26] T. Kundu, J. Bereiter-Hahn, and K. Hillmann, "Measuring elastic properties of cells by evaluation of scanning acoustic microscopy $V(z)$ values using simplex algorithm," *Biophys. J.*, vol. 59, pp. 1194–1207, Jun. 1991.
[27] T. Kundu, J. Bereiter-Hahn, and K. Hillmann, "Calculating acoustical properties of cells—Influence of surface-topography and liquid layer between cell and substrate," *J. Acoust. Soc. Am.*, vol. 91, pp. 3008–3017, May 1992.
[28] H. Okawai, M. Tanaka, and F. Dunn, "Noncontact acoustic method for the simultaneous measurement of thickness and acoustic properties of biological tissues," *Ultrasonics*, vol. 28, pp. 401–410, Nov. 1990.
[29] C. S. Jorgensen, J. M. Hasenkam, and T. Kundu, "Measurement of material properties of hard and soft biological tissues by means of $V(z)$ and $V(f)$ curves obtained with acoustic microscopy," *Proc. SPIE*, vol. 4335, pp. 244–253, 2001.
[30] H. K. Graham, R. Akhtar, C. Kridiotis, B. Derby, T. Kundu, A. W. Trafford, and M. J. Sherratt, "Localised micro-mechanical stiffening in the ageing aorta," *Mech. Ageing Dev.*, vol. 132, no. 10, pp. 459–467, 2011.
[31] R. G. Maev and K. I. Maslov, "Temperature effects in the focal region of the acoustic microscope," *IEEE Trans. Ultrason. Ferroelectr. Freq. Control*, vol. 38, pp. 166–171, May 1991.
[32] T. Kujawska, J. Wojcik, and L. Filipczynski, "Possible temperature effects computed for acoustic microscopy used for living cells," *Ultrasound Med. Biol.*, vol. 30, pp. 93–101, Jan. 2004.
[33] E. C. Weiss, P. Anastasiadis, G. Pilarczyk, R. M. Lemor, and P. V. Zinin, "Mechanical properties of single cells by high-frequency time-resolved acoustic microscopy," *IEEE Trans. Ultrason. Ferroelectr. Freq. Control*, vol. 54, pp. 2257–2271, Nov. 2007.
[34] J. Lubbers and R. Graaff, "A simple and accurate formula for the sound velocity in water," *Ultrasound Med. Biol.*, vol. 24, pp. 1065–1068, Sep. 1998.
[35] K. Raum, K. V. Jenderka, A. Klemenz, and J. Brandt, "Multilayer analysis: Quantitative scanning acoustic microscopy for tissue char-

acterization at a microscopic scale," *IEEE Trans. Ultrason. Ferroelectr. Freq. Control*, vol. 50, pp. 507–516, May 2003.
[36] T. Grandke, "Interpolation algorithms for discrete Fourier-transforms of weighted signals," *IEEE Trans. Instrum. Meas.*, vol. 32, no. 2, pp. 350–355, 1983.
[37] V. K. Jain, W. L. Collins, and D. C. Davis, "High-accuracy analog measurements via interpolated FFT," *IEEE Trans. Instrum. Meas.*, vol. 28, no. 2, pp. 113–122, 1979.
[38] C. M. Moran, N. L. Bush, and J. C. Bamber, "Ultrasonic propagation properties of excised human skin," *Ultrasound Med. Biol.*, vol. 21, no. 9, pp. 1177–1190, 1995.
[39] F. A. Duck, *Physical Properties of Tissue. A Comprehensive Reference Book*. London, UK: Academic Press, 1990.
[40] A. G. Every, K. Hillmann, K. U. Wurz, H. Hasselmann, and W. Grill, "Singularities in surface acoustic microscopy phase images," *Physica B*, vol. 220, pp. 714–716, Apr. 1996.
[41] Y. Sasaki, T. Endo, T. Yamagishi, and M. Sakai, "Thickness measurement of a thin-film layer on an anisotropic substrate by phase-sensitive acoustic microscope," *IEEE Trans. Ultrason. Ferroelectr. Freq. Control*, vol. 39, pp. 638–642, Sep. 1992.

Xuegen Zhao received his B.Sc. and M.Sc. degrees in physics from Shandong University, China, in 1987 and 1990, respectively. He was then based at the Institute of Physics in Beijing, where he was awarded a Ph.D. degree in physics in 1993. He joined Professor Derby's research group at The University of Manchester in 2008 to develop techniques for mechanical characterization of soft biological tissues using scanning acoustic microscopy. Prior to this, he was working on the characterization and application of functional magnetic materials, in particular magnetostrictive materials, at the University of Salford, where he had been based since 1996.

Riaz Akhtar graduated from UMIST in 2003 with a First Class M.Eng. (Hons) degree in biomedical materials science with industrial experience. In 2007, he completed a Ph.D. degree at The University of Manchester on the micromechanical behavior of bone. Following this, he undertook a postdoctoral position investigating the micromechanical properties of soft tissue. In July 2008, Riaz was awarded a British Heart Foundation Advanced Training fellowship investigating vascular stiffening and diabetes. He joined the University of Liverpool in October 2011 as a lecturer in Biomedical Engineering.

Nadja Nijenhuis graduated from the University of Amsterdam in experimental physics with an M.Sc. degree. She worked on the micromechanical properties of the pericellular matrix with a focus on the macromolecule hyaluronan, as part of her Ph.D. studies at the University of Amsterdam, The Netherlands (2003–2007) and the Georg-August University of Göttingen, Germany (2008). She joined Professor Derby's research group at The University of Manchester in 2009, studying cell mechanics with scanning acoustic microscopy.

Steven Wilkinson graduated from Heriot-Watt University with a B.Sc. (Hons) degree in optoelectronics and laser engineering in 1993. In 2002, he was awarded a Ph.D. degree from Aberdeen University in biomedical physics. During and following his Ph.D. studies, Steve gained experience in many different imaging and research areas. He also worked at the Osteoporosis Research Unit in Aberdeen from 1998 to 2002. In 2003, he took a position working on small angle diffraction imaging of connective tissue based at the synchrotron radiation source (SRS), Daresbury Laboratory. In 2008, he joined Professor Derby's group to work on developing acoustic microscopy methods for characterizing soft biological tissues.

Lilli Murphy's photograph and biography were unavailable at time of publication.

Christoph Ballestrem graduated from University of Constance, Germany, in 1996 and then completed a Ph.D. degree in 2000 at the University of Geneva, Switzerland. He was a postdoctoral fellow at the Technical University of Dresden, Germany (2000–2001) and then at the Weizmann Institute of Science, Israel (2001–2004), supported by Feinberg Graduate School and Minerva fellowships. He joined The University of Manchester as a Wellcome Trust Research Fellow in 2004 and was then appointed as a lecturer in 2007 within the Wellcome Trust Centre for Cell-Matrix Research.

Michael Sherratt is a member of the School of Biomedicine at the University of Manchester and a former Age UK Senior Research Fellow. He received his B.Sc. Hons (biology) and Ph.D. degrees from the University of Manchester and an M.Sc. degree from UMIST. Michael serves as Treasurer for the British Society for Research on Ageing and as Director of the University of Manchester Biological Atomic Force Microscopy Facility. His research is focused on the effects of ageing and disease on the structure and mechanical function of dynamic tissues (including skin, blood vessels, and the intervertebral disc) at molecular to whole organ length scales.

Rachel Watson is a Non-Clinical Senior Lecturer in Aesthetic Dermatology within the School of Translational Medicine, The University of Manchester. She received her B.Sc. (anatomy and cell biology) and Ph.D. degrees from the University of Sheffield. She sits on the editorial boards of 3 scientific journals and is Co-Editor of *Clinical & Experimental Dermatology*. Rachel also sits on the Executive Committee of the British Society for Investigative Dermatology (since 2006). Her research includes understanding the mechanisms that lead to skin aging and the assessment of extracellular matrix repair, particularly by topical retinoids.

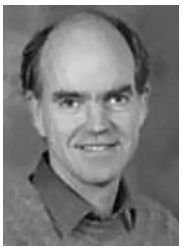

Brian Derby graduated in Natural Sciences from Cambridge University in 1978 and obtained his Ph.D., also from Cambridge, in 1981. He spent 1 year working at the Centre d'Etudes Nucleaire de Grenoble as an ESA Fellow before spending 2 years in the Cambridge University Engineering Department as a Research Fellow. He was in the University of Oxford, Department of Materials from 1983 to 1998 as a Research Fellow, Lecturer, and Reader in Materials Engineering, where he was Director of the Oxford Centre for Advanced Materials and Composites. He was appointed Professor in Materials Science at The University of Manchester in 1999. He was elected a member of the World Academy of Ceramics in 2004.